Available online at www.sciencedirect.com
ScienceDirect
Acta Materialia 55 (2007) 2129–2135
Acta MATERIALIA
www.actamat-journals.com

Determination of the local environment of silicon and the microstructure of quaternary CrAl(Si)N films

J.L. Endrino [a], S. Palacín [b], M.H. Aguirre [c], A. Gutiérrez [b,*], F. Schäfers [d]

[a] Lawrence Berekeley National Laboratory, Berkeley, CA 94720, USA
[b] Departamento de Física Aplicada, Universidad Autónoma de Madrid, 28049 Madrid, Spain
[c] Swiss Federal Laboratories for Material Testing and Research (EMPA), 129 Ueberlandstrasse, CH-8600 Duebendorf, Switzerland
[d] BESSY GmbH, Albert-Einstein-Straße 15, 12489 Berlin, Germany

Received 11 July 2006; received in revised form 3 November 2006; accepted 5 November 2006
Available online 26 January 2007

Abstract

Nanocomposite CrAlSiN compounds prepared by the cathodic arc evaporation technique were subjected to structural and mechanical characterization tests. X-ray diffraction, X-ray absorption spectroscopy (XAS) and transmission electron microscopy (TEM) were employed to investigate the effects of Si addition on the structure and phase development of the metastable NaCl structure of high aluminum CrAlN films. TEM studies revealed that partial substitution of the metal component by Si in CrAlN results in the nucleation of a wurtzite h-AlN phase even for amounts of silicon as low as ~2–3 at.%. XAS measurements at the Cr and Si K-edges indicated that the local environment of Cr atoms is strongly affected by the Si addition, and that silicon may also be part of the crystalline phase. These results indicate the formation of complex Cr–Si–X compounds, where X can be N, Al or both, and the formation of composite nanocrystalline CrAlSiN films.

Keywords: Physical vapor deposition; Transmission electron microscopy; X-ray absorption spectroscopy; Nitrides; Nanocrystalline microstructure

1. Introduction

Changes in the structure and chemistry of Si-containing coatings as compared with those without Si can influence phase formation, grain size and mechanical properties of hard nitride films [1–3]. Adding silicon to transition metal nitrides (MeN) has been reported to significantly improve several mechanical properties, including hardness, toughness and oxidation resistance, which are desirable qualities in most wear-resistant coatings [4,5]. Most microstructural studies of Si-containing nitrides report the formation of two-phase nanocomposite systems composed of nanocrystalline MeN grains embedded in an amorphous silicon nitride (*a*-Si:N) matrix [1,4–6]. The low solubility of silicon in the lattice of B1-structured nitrides has been explained by the higher mixing enthalpy of complex ternary nitride compounds when compared with the lower free energy of MeN and a-Si_3N_4 phases [4]. Recent structural studies of TiSiN films have pointed out the possibility of large amounts of Si dissolution into TiN grains when the films are grown by physical vapor deposition at relatively low deposition temperatures [7,8]. However, the authors of these studies could not provide proof of the formation of a TiSiN solid solution phase based only in X-ray diffraction (XRD) and transmission electron microscopy (TEM) experiments. Recently, Meng et al. [2,9] performed detailed examinations of the microstructure of Ti–Si–N films by combining both TEM and X-ray absorption spectroscopy (XAS) techniques. In this case, the gradual changes observed in the Si K-edge spectra as a function of the Si content along with TEM observations of columnar nanometer-scale B1-TiN domains provided evidence of dissolution of Si within the TiN phase.

However, the most commonly employed element to alloy MeN films for mechanical applications is aluminum.

* Corresponding author.
E-mail address: a.gutierrez@uam.es (A. Gutiérrez).

1359-6454/$30.00
doi:10.1016/j.actamat.2006.11.014

Many studies have shown that Al-containing nitride coatings, such as TiAlN and most recently CrAlN, provide excellent wear protection at high service temperature [10–12]. The high thermal stability, excellent hot hardness and good oxidation resistance of NaCl-structure metal aluminum nitride (MeAlN) is due to the nucleation of a metastable c-AlN at high temperatures and the resultant formation of alumina-like films at high temperatures in the presence of oxygen [13]. The solubility of aluminum in NaCl-structured MeAlN is limited. In $Ti_{1-x}Al_xN$ and $Cr_{1-x}Al_xN$ systems, studies have shown that the maximum solubility of aluminum before the formation of the hexagonal wurtzite-type AlN is for x between 0.6 and 0.7 [14,15]. Supersaturated metastable MeAlN films have recently drawn a lot of attention due to the high hardness of the B1-structure and maximum aluminum content. Similarly, it is known that quaternary Ti–Al–Si–N compounds can provide further improvement in the mechanical properties of MeN [16–21]. However, there is a lack of detailed studies about the local chemical environment of silicon and the nanostructures formed in the deposition of complex quaternary nitrides.

In this present work, the structural effects of Si substitution of chromium in supersaturated metastable CrAlN coatings were analyzed by XRD, TEM and XAS. The last proved to be a very appropriate tool for this kind of study because of its high sensitivity to the atom local environment, which allowed the determination of the degree of dissolution of Si atoms in CrAlN grains.

2. Experimental details

The CrAlSiN films investigated in this research were deposited using a Balzers' rapid coating system (RCS) deposition machine in a cathodic arc ion-plating mode. Customized CrAl(30:70), CrAlSi(25:70:5), CrAlSi(20:70:10) and CrAlSi(15:70:15) targets in a reactive nitrogen atmosphere were used to obtain coatings with a variable Al/Cr ratio and increasing Si content. Mirror-polished squared cemented carbide inserts were used as substrates, the temperature of which was held at approximately 500 °C during deposition. The thickness of all the coating samples was within 3.5 ± 0.2 μm. A Siemens D500 diffractometer with a Cu $K\alpha$ tube and the $\theta/2\theta$ mode was used to perform XRD analysis and identify the phases formed. Chemical analysis was performed on a field emission scanning electron microscope (LEO 1550 FEG) equipped with INCA energy dispersive spectroscopy (EDS). The results are shown in Table 1. Discs (3 mm diameter) of the coating/substrate, in planar view geometry, were cut by spark erosion machine and mechanically polished from the substrate up to 100 μm thickness. The Ar^+ ion milling equipment (Precision Ion Polishing System-GATAN 691) was used to thin the discs down to electron transparency.

Table 1
Composition analyzed by EDS-SEM in situ

Sample	Target nominal composition	Cr (at.%)	Al (at.%)	Si (at.%)
1	Cr/Al (30:70)	32.5	67.5	–
2	Cr/Al/Si (25:70:5)	27.6	67.8	4.6
3	Cr/Al/Si (20:70:10)	23.1	67.6	9.3
4	Cr/Al/Si (15:15:70)	17.5	68.1	14.4

Diffraction patterns and low- and high-resolution images were obtained using a Tecnai F30 electron microscope working at 300 kV.

XAS measurements of the Cr and Si K-edges were carried out at the KMC-1 beamline of the BESSY synchrotron facility, with double crystal monochromator, using a standard chamber equipped with a high-resolution solid-state fluorescence detector.

3. Results and discussion

3.1. X-ray diffraction

XRD patterns of all the deposited samples are shown in Fig. 1. Sample 1 (0 rel. at.% Si) shows a well-defined polycrystalline B1 (NaCl-type) microstructure with a strong (1 1 1) preferred orientation. The peaks fall between those for B1 aluminum nitride Joint Committee Powder Diffraction Standard (JCPDS) Card No. 24-1495 and B1 chromium nitride (JCPDS Card No. 11-0065), which implies complete solubility of chromium, aluminum and nitrogen in the rock-salt-type lattice even when the measured relative aluminum content was near 68 at.% (Table 1), in

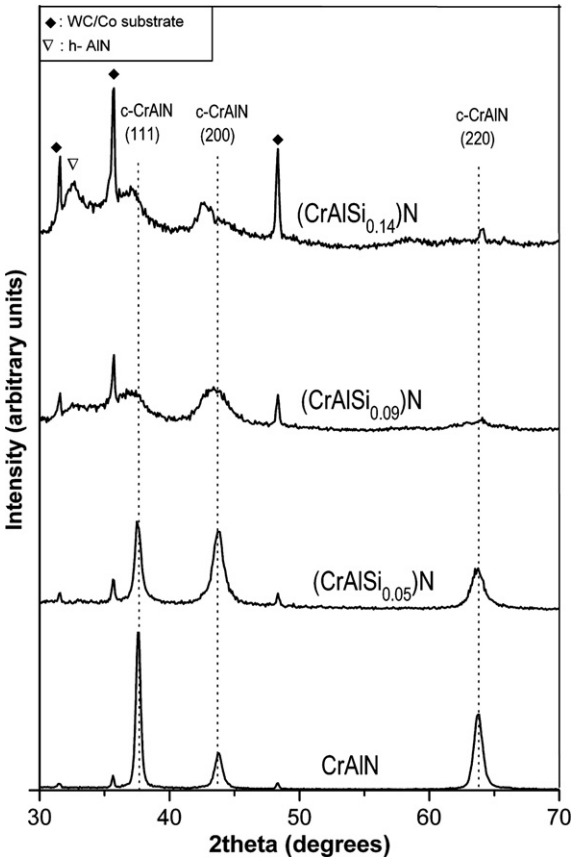

Fig. 1. XRD patterns for CrAl(Si)N thin films compared with CrAlN.

accordance with numerous studies which show that higher aluminum contents in $Cr_{1-x}Al_xN$ result in the nucleation of the wurtzite hexagonal close-packed (hcp)-AlN [14,22]. Sample 2 (5 rel. at.% Si) appeared to maintain the same B1 structure as sample 1 (0 rel. at.% Si). In comparison with sample 1, the diffraction pattern indicated that the silicon-containing sample is less textured (the diffraction ratio (200)/(111) was about 0.9) and has a lower degree of crystallinity. Samples 3 and 4 (which contained larger amounts of silicon) showed only amorphous peaks in (111) and (200) planes marked for the cubic c-CrAlN of sample 1. The diffraction pattern for sample 4 (14 rel. at.% Si) also showed a peak at $2\theta \sim 32.3°$, which is consistent with the $(001)_{hex}$ plane for wurtzite hcp-AlN (JCDPS Card No. 08-0262).

3.2. Transmission electron microscopy

TEM images and electron diffraction patterns in plane-view geometry are shown in Fig. 2a and b for: $(Cr_{0.3}Al_{0.7})N$ and (c) and (d) $(Cr_{0.25}Al_{0.7}Si_{0.05})N$, sample 1 and sample 2, respectively, described in Table 1. Tables 2 and 3 describe

Table 2
Theoretical and experimental values for dhkl of CrAlN

Ring No.	hkl	Theoretical d_{hkl} (Å)	Experimental d_{hkl} (±0.05) Å
1	111	2.41	2.41
2	200	2.09	2.06
3	220	1.47	1.46
4	311	1.26	1.45
5	222	1.20	1.18
6	400	1.04	1.03
7	420	0.94	0.92
8	422	0.85	0.84

ring diffraction patterns of both samples, respectively. There exist markedly differences between ring diffraction patterns of both samples comparing Fig. 2a and c. This difference can be seen only in electron diffraction due to the local character of the analysis in TEM method compared with the XRD. Sample 1 (0 rel. at.% Si) shows sharp diffraction spots arranged in a circle, as usual for polycrystalline materials, while sample 2 (5 rel. at.% Si) shows a larger number of diffraction rings than sample 1 and diffuse scattering, producing a continuous ring pattern. The presence

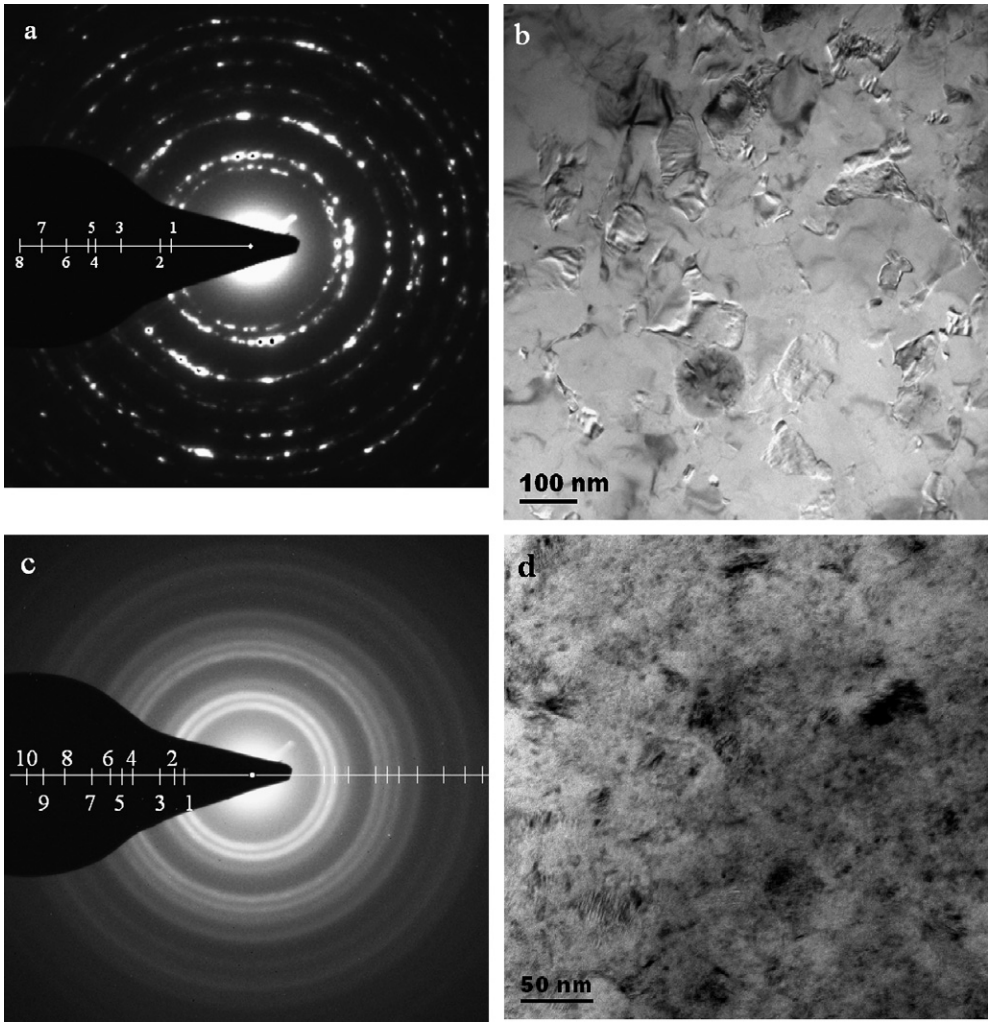

Fig. 2. Electron diffraction patterns and TEM images in plane-view geometry for: (a), (b) $(Cr_{0.3}Al_{0.7})N$ and (c), (d) $(Cr_{0.25}Al_{0.7}Si_{0.05})N$, respectively.

Table 3
Interplanar distances for CrAlSiN (cubic structure) and AlN (hexagonal structure)

Ring No.	Experimental d_{hkl} Å ± 0.05Å	$CrAlSiN_{cub}$ $a = 4.18$ Å hkl	AlN_{hex} $a = 3.11$ Å, $c = 4.98$ Å hkl
1	2.70		100
2	2.40	111	
3	2.05	200	
4	1.59		110
5	1.45	220	
6	1.34		200
7	1.12		104
8	1.03	400	203
9	0.91	420	211
10	0.84	422	

of more diffraction rings in the diffraction pattern of the second sample is because there are two structures and/or phases coexisting, corresponding to CrAl(Si)N (cubic) and AlN (hexagonal). The continuous ring pattern instead of sharp spots is a consequence of the fine and small size grains distribution in sample 2 (5 rel. at.% Si), while the diffuse scattering is due to the presence of an amorphous region in the sample. In spite of the different magnification of micrographs in Fig. 2b and d, the morphology of the CrAlN and CrAl(Si)N polycrystals are quite different, since CrAlN grains are bigger and more crystalline than the compound with Si added. The amorphous zone, seen through the diffuse scattering in Fig. 2d, is due to the possible formation of SiO_x compounds in sample 2 (5 rel. at.% Si) [18]. Even though there is no evidence for the presence of a SiN_x phase in the experimental diffraction pattern (showed in Fig. 2c), the careful analysis of Fig. 3c in the fast Fourier transform (FFT) shows some diffuse traces (at around 6–7 Å) from a possible SiN_x compound at a very local level, i.e. on the scale of a few nanometers.

The study by high-resolution TEM (HRTEM) of the sample 1 (CrAlN) compound confirms the cubic (NaCl-type) structure proposed. Fig. 3a shows small grains near the exact Bragg condition along the zone axis [1 1 0], but the surrounding grains do not meet the Bragg condition and only the interplanar spacing is resolved. This plane distance corresponds to $d_{002} \approx 2.05$ Å.

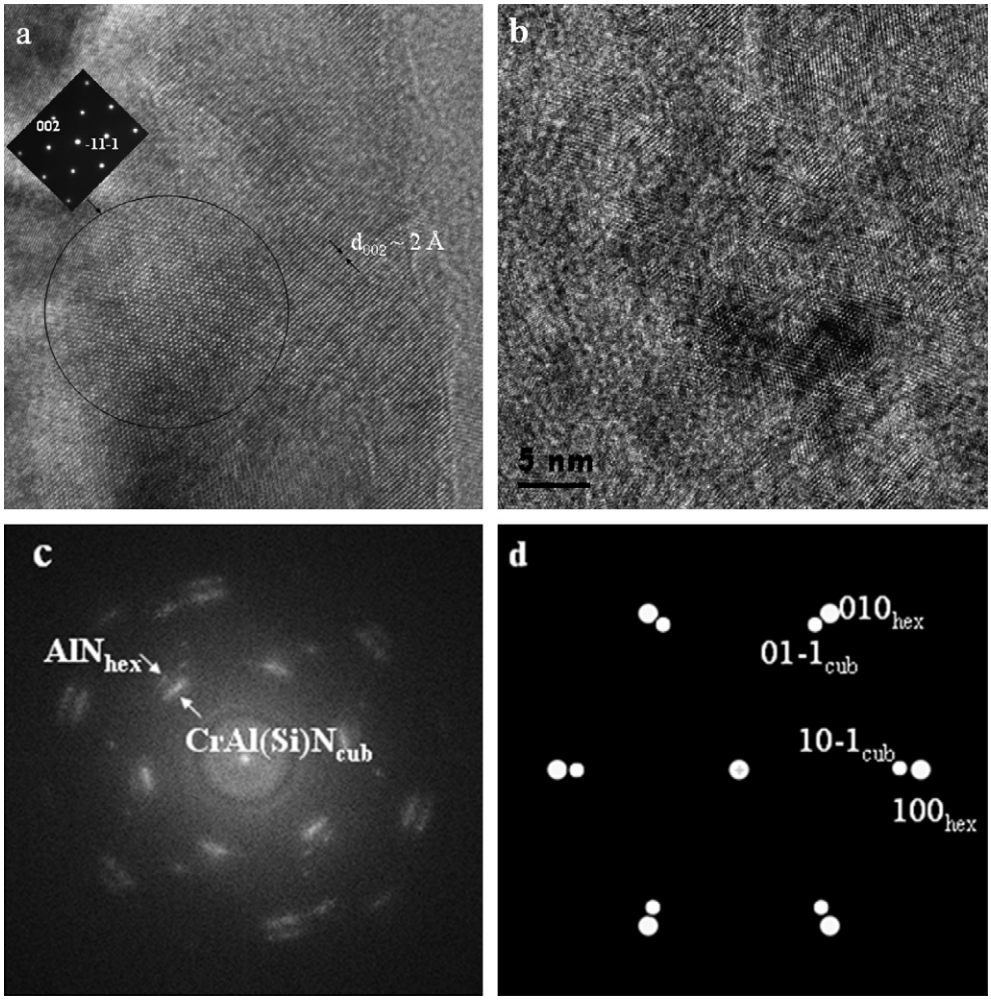

Fig. 3. (a) HRTEM image and (inset) diffraction pattern of CrAlN (sample 1) in [1 1 0] oriented grain. (b) HRTEM image of $CrAlSi_{0.05}N$ (sample 2). (c) FFT showing the presence of two overlapping structures, hexagonal ([0 0 1] zone axis of AlN) and cubic ([1 1 1] zone axis of CrAl(Si)N). (d) Simulated FFT with cubic and hexagonal overlapped structures of both compounds.

A HRTEM image of sample 2 (5 rel. at.% Si) (Fig. 3b) shows the amorphous background between small particles and the coherence between the $(0\,0\,1)_{hex}$ and $(1\,1\,1)_{cub}$ planes. The lattice parameter of CrAlSiN is $a \approx 4.18 \pm 0.05$ Å, and for AlN $a \approx 3.11$ Å, $c \approx 4.98$ Å. There is no meaningful change in the lattice parameter with the addition of 5 at.% of Si, only a small expansion in the cubic cell parameter, which is hardly detected by TEM. The high-resolution image represents the projected potential of the structure of different nanograins in different orientations on an amorphous background. The sizes of the grains are between 5 and 10 nm. As we remarked above, the amorphous background can be attributed to the presence of Si. Silicon becomes unstable under the thinning process by Ar-ion milling, and the electron beam in TEM easily converts the region analyzed into an amorphous zone [23]. The velocity of this reaction is increased if oxygen and/or nitrogen are present, as was the case for the samples analyzed; the main reason for this is the formation of amorphous SiO_x and possibly SiN_x.

FFT analysis of the image in Fig. 3c shows the presence of two diffraction patterns overlapping, one corresponding to the [1 1 1] zone axis of CrAlSiN (cubic structure) and the second to the [0 0 1] zone axis of AlN (hexagonal structure). This orientation relationship, (0 0 1)hex//{1 1 1} cub, is very common between precipitates and matrix with hexagonal and cubic structures, respectively. The diffraction of each variant (0 0 1)hex//{1 1 1} cub produces reflections in identical direction but with different indexing, because of the six- and threefold symmetry of $[0\,0\,1]_{hex}$ and $[1\,1\,1]_{cub}$ poles (see the simulation in Fig. 3d). The reflections do not overlap because of different lattice parameters: $d_{0\,1\,-1} \approx 2.8$ Å in cubic CrAlSiN and $d_{1\,0\,0} \approx 2.69$ Å in hexagonal AlN. That is, there are present in sample 2 two different crystalline phases, AlN and CrAlSiN, but the exact composition is not possible to determine by EDS in situ due to the short range order of the fine grains. Another problem is the presence of an amorphous region in between, i.e. SiO_x and SiN_x compounds, which overlaps the nanocrystalline compounds.

3.3. X-ray absorption spectroscopy

Fig. 4 shows XAS spectra at the Cr K-edge of CrAlSiN samples with different Si content. The pre-edge region, at 5960 eV, is associated with transitions from Cr-1s states to Cr-3d states hybridized with 2p empty states of the ligand atoms. This hybridization allows 1s3d transitions, which are otherwise dipole forbidden. The XAS spectrum of the CrAlN sample (sample 1) shows a tiny pre-edge peak at this position, very similar to that reported in previous works for Cr_2O_3 [24–26], suggesting that Cr in this compound is in the form of Cr^{3+}. The intensity of this peak slightly increases for sample 2, with a Si content of 5%, whereas for samples 3 and 4 (9% and 14% Si, respectively) the increase is significantly larger. The increase of this feature has been explained in the case of oxide compounds in terms of a valence increase (from +3 to +4, +5 or +6) [24,26,27], or in terms of a reduction of crystalline domains down to the nanoscale [25]. The presence of high valence Cr would involve a shift to higher energies of the main absorption edge, which we do not observe in our samples, so we can exclude the presence of this kind of Cr compounds. The only explanation for the observed intensity increase in samples 3 and 4 must include a chemical interaction between Si and Cr, which would give rise to Cr-3d Si-2p hybridization. Consequently, the peak at 5960 eV can be assigned to transitions from Cr-1s states to Cr-3d states hybridized with Si-2p empty states. In addition to this pre-edge intensity increase, the addition of Si produces a smoothening of the overall spectral lineshape, which points towards an amorphization of the Cr-containing compounds structure.

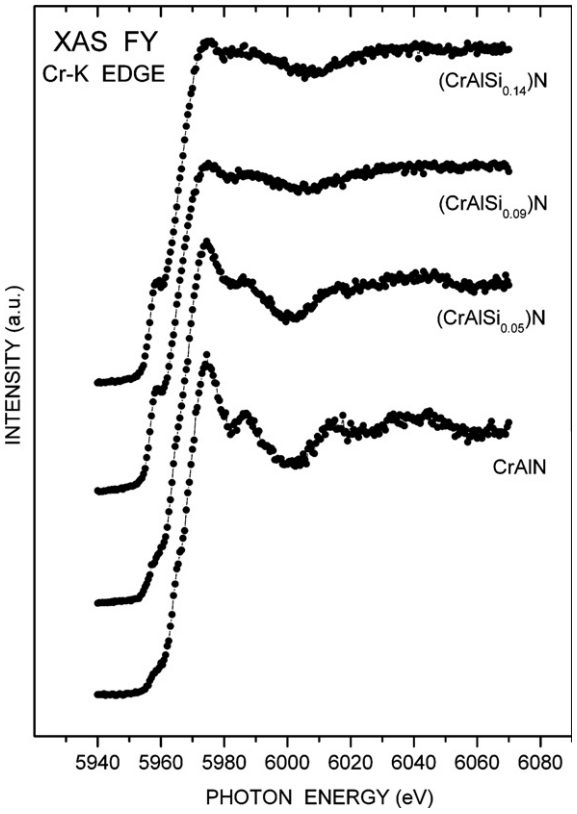

Fig. 4. X-ray absorption spectra in fluorescence yield mode at the Cr K-edge for several CrAl(Si)N coatings.

Fig. 5 shows XAS spectra at the Si K-edge of CrAlSiN samples with different Si content, as well as pure Si and SiO_2 single crystals and an amorphous Si_3N_4 as reference samples. From a comparison of the CrAlSiN spectra with that of pure Si, we can exclude that Si incorporates CrAlN as an atomic solid solution, because the spectra would resemble that of pure Si. The spectrum for sample 2, with 5% Si (bottom), has a peak at 1847 eV, which is aligned with feature (c) of the spectrum for the SiO_2 single crystal. This indicates that at low Si content there is some oxygen contamination in the form of SiO_2. Additionally, the edge positions at 1842 eV, as well as the peak observed at

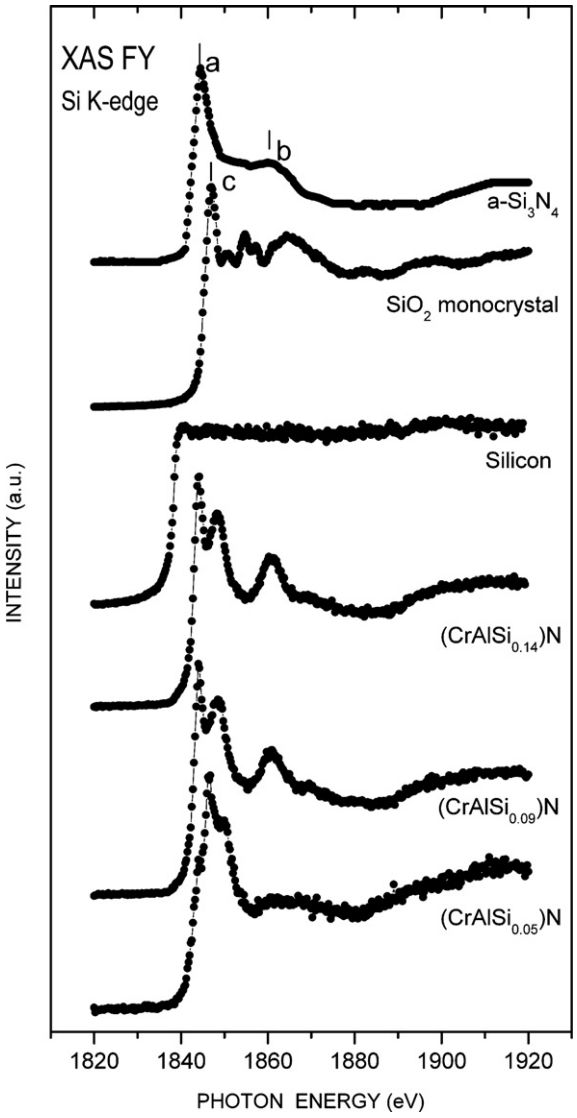

Fig. 5. X-ray absorption spectra in fluorescence yield mode at the Si K-edge for several CrAlSiN coatings. Additionally, Si K-edge spectra for Si, SiO_2 and a-Si_3N_4 are shown for reference.

1850 eV, are evidence for the presence of Si–N compounds in this sample. The feature assigned to SiO_2 disappears for samples with higher Si content. The spectra for samples with 9% and 14% Si are very similar, with a main peak at 1844 eV. This energy position corresponds to the main peak observed for Si_3N_4, suggesting that Si is in the form of some nitride compound. However, the more complex spectral lineshape, as compared with that of Si_3N_4, could be an evidence of the formation of some ternary Si–N–X compound. By bringing together both Cr–K and Si–K XAS spectra, it seems clear that there are two different pictures: samples with the highest Si content (9% and 14%) show a similar behavior, with the amorphization of the Cr-based crystal structure, probably as CrAl(Si)N, and the formation of Si–N–X complex compounds, where X accounts for Cr, Al or both. On the other hand, the sample with the lowest Si content (5%) does not show so drastic changes, being Si incorporated probably as a Si–N solid solution into the CrAlN structure, and with some SiO_2 contamination.

4. Conclusions

In summary, we have combined XRD, TEM and XAS techniques to perform a detailed examination of the microstructure of quaternary CrAl(Si)N films, where Si atoms strive to replace Cr in a metastable B1-NaCl crystal structure. XRD results showed that the B1-textured monolithic structure of CrAlN become less textured with small amounts of added Si and amorphous with hexagonal AlN precipitates with high amounts of Si. Both XRD and TEM showed that Si has a grain refining effect in the CrAlN films. Localised electron diffraction patterns in plane-view geometry of the sample with the smallest amount of Si content (5 at.%) showed the presence of multiple diffraction rings, indicating the coexistence of two crystalline phases, possibly corresponding to CrAl(Si)N (cubic) and AlN (hexagonal). FFT analysis and HRTEM were used to unequivocally confirm the presence of h-AlN phase even for the sample with the lowest amounts of Si. Analysis of the Cr K-edge XAS data showed that Si produced a smoothening of the spectral lineshape, which is an indication of amorphization of the Cr-containing compounds. The similar and complex shape of Si K-edge spectrum for samples with 9 and 14 rel. at.% of Si suggests that silicon forms some ternary Si–N–X compound, with X being Cr or Cr and Al. Both XAS and TEM techniques detected the presence of an amorphous a-SiO_2 phase for the sample with the lowest amount of Si.

Acknowledgments

The technical assistance of R. Mitdank during X-ray fluorescence measurements at BESSY is gratefully acknowledged. The authors would also like to thank to the Centre of Microscopy EMEZ-ETH Zurich by providing electron microscopy facilities. One of the authors (A.G.) thanks financial support from the Spanish MEC through "Ramón y Cajal" and BFM2003-03277 contracts, as well as from the UE through RII3-CT-2004-506008 contract.

References

[1] Martin PJ, Bendavid A, Cairney JM, Hoffman M. Surf Coat Technol 2005;200:2228.
[2] Meng WJ, Zhang XD, Shi B, Jiang JC, Rehn LE, Baldo PM, et al. Surf Coat Technol 2003;163–164:251.
[3] Zhang XD, Meng WJ, Wang W, Rehn LE, Baldo PM, Evans RD. Surf Coat Technol 2004;177–178:325.
[4] Veprek S. Thin Solid Films 1998;317:449.
[5] Veprek S, Argon AS. Surf Coat Technol 2001;146–147:175.
[6] Watanabe H, Sato Y, Nie C, Ando A, Ohtani S, Iwamoto N. Surf Coat Technol 2003;169–170:452.
[7] Shalaeva EV, Borisov SV, Denisov OF, Kuznetsov MV. Thin Solid Films 1999;339:129.

[8] Vaz F, Rebouta L, Almeida B, Goudeau P, Pacaud J, Riviere JP, et al. Surf Coat Technol 1999;120–121:166.
[9] Meng WJ, Zhang XD, Shi B, Tittsworth RC, Rehn LE, Baldo PM. J Mater Res 2002;17:2628.
[10] Endrino JL, Derflinger V. Surf Coat Technol 2005;200:988.
[11] Endrino JL, Fox-Rabinovich GS, Gey C. Surf Coat Technol 2006;200:6840.
[12] Fox-Rabinovich GS, Veldhuis SC, Scvortsov VN, Shuster LS, Dosbaeva GK, Migranov MS. Thin Solid Films 2004;469–470:505.
[13] Fox-Rabinovich GS, Beake BD, Endrino JL, Veldhuis SC, Parkinson R, Shuster LS, et al. Surf Coat Technol 2006;200:5738.
[14] Willmann H, Mayrhofer PH, Persson POA, Reiter AE, Hultman L, Mitterer C. Scripta Mater 2006;54:1847.
[15] Kimura A, Kawate M, Hasegawa H, Suzuki T. Surf Coat Technol 2003;169–170:367.
[16] Carvalho S, Ribeiro E, Rebouta L, Pacaud J, Goudeau P, Renault PO, et al. Surf Coat Technol 2003;172:109.
[17] Holubar P, Jilek M, Sima M. Surf Coat Technol 1999;120–121:184.
[18] Li YS, Shimada S, Kiyono H, Hirose A. Acta Mater 2006;54:2041.
[19] Nakonechna O, Cselle T, Morstein M, Karimi A. Thin Solid Films 2004;447–448:406.
[20] Parlinska-Wojtan M, Karimi A, Coddet O, Cselle T, Morstein M. Surf Coat Technol 2004;188–189:344.
[21] Tanaka Y, Ichimiya N, Onishi Y, Yamada Y. Surf Coat Technol 2001;146–147:215.
[22] Brecher C, Spachtholz G, Bobzin K, Lugscheider E, Knotek O, Maes M. Surf Coat Technol 2005;200:1738.
[23] Schuhrke T, Mandl M, Zweck J, Hoffmann H. Ultramicroscopy 1992;41:429.
[24] Berry AJ, O'Neill HStC. Am Mineral 2004;89:790.
[25] Hwang S-J, Park H-S, Choy J-H. Solid State Ionics 2002;151:275.
[26] Pantelouris A, Modrow H, Pantelouris M, Hormes J, Reinen D. Chem Phys 2004;300:13.
[27] Jousseaume C, Ribot F, Kahn-Harari A, Vivien D, Villain F. Nucl Instrum Meth Phys Res Sect B: Beam Interact Mater Atoms 2003;200:425.